HHS Public Access

Author manuscript

Neuron. Author manuscript; available in PMC 2018 February 08.

Published in final edited form as:

Neuron. 2017 February 08; 93(3): 606–615.e3. doi:10.1016/j.neuron.2016.12.020.

Glut4 mobilization supports energetic demands of active synapses

Ghazaleh Ashrafi[1], **Zhuhao Wu**[2], **Ryan J. Farrell**[1,2], and **Timothy A. Ryan**[1]

[1]Department of Biochemistry, Weill Cornell Medicine, New York, New York 10021, USA

[2]Laboratory of Brain Development and Repair, The Rockefeller University, New York, NY 10065, USA

SUMMARY

The brain is highly sensitive to proper fuel availability as evidenced by the rapid decline in neuronal function during ischemic attacks and acute severe hypoglycemia. We previously showed that sustained presynaptic function requires activity-driven glycolysis. Here, we provide strong evidence that during action potential (AP) firing, nerve terminals rely on the glucose transporter Glut4 as a glycolytic regulatory system to meet the activity-driven increase in energy demands. Activity at synapses triggers insertion of Glut4 into the axonal plasma membrane driven by activation of the metabolic sensor AMP kinase. Furthermore, we show that genetic ablation of Glut4 leads to an arrest of synaptic vesicle recycling during sustained AP firing, similar to what is observed during acute glucose deprivation. The reliance on this biochemical regulatory system for "exercising" synapses is reminiscent of that occurring in exercising muscle to sustain cellular function, and identifies nerve terminals as critical sites of proper metabolic control.

INTRODUCTION

Regulatory metabolic pathways ensure fuel availability for the proper function of various body tissues. These pathways are particularly important for organs that undergo rapid changes in metabolic demand such as striated muscle and brain. The brain, while only representing ~ 2.5% of body mass, accounts for ~20% of energy expenditure, and like the heart, is never in a fully "resting" state, undergoing rapid local changes in activity. In order to maintain function, such changes in activity must be accompanied by a corresponding upregulation of fuel availability. Not surprisingly, cognitive function is closely linked to the metabolic state of the brain: acute interruptions in fuel supply, as experienced by neurons

Lead Contact: T.A.R. (taryan@med.cornell.edu).

AUTHOR CONTRIBUTIONS

T.A.R. and G.A. designed the study. GA performed the experiments with the exception of the brain slice immunostaining carried out by Z.W and R.J.F in the laboratory of Marc Tessier Lavigne (Rockefeller University). T.A.R. and G.A. wrote the manuscript.

SUPPLEMENTARY INFORMATION

Supplementary figures S1-S6 and their figure legends are attached as separate files.

during ischemic events or bouts of hyperglycemia, generally lead to profound and immediate suppression of neuronal function. These examples underscore the general vulnerability of brain function to the maintenance of proper metabolic support and illustrate the need to dissect how neuronal activity regulates fuel usage and availability. The biochemical mechanisms responsible for regulating fuel availability in neurons however are poorly understood and have likely been obscured by the fact that chronic genetic ablation of fuel delivery pathways often result in maladaptive compensations (Abel et al., 1999). We recently showed that electrical activity at nerve terminals drives new glycolysis that is required to sustain synaptic vesicle (SV) recycling (Rangaraju et al., 2014). Glucose is the main energy source of the brain and nerve terminals are enriched in the machinery for glycolysis as 5 of the 10 essential glycolytic enzymes co-purify with SVs (Ikemoto et al., 2003; Knull and Fillmore, 1985). Moreover, recent *in-vivo* studies have shown that a local glycolytic "metabolon" forms in nerve terminals during energy deprivation and neuronal activity (Jang et al., 2016). However, the cellular and molecular mechanism by which activity drives nerve terminal glycolysis is unknown. It has long been known that exercise increases glucose uptake in muscle compared to at rest (Chauveau, 1887) by contraction-driven insertion of the glucose transporter Glut4 into the plasma membrane (Douen et al., 1990; Lauritzen et al.; Roy and Marette, 1996) through a mechanism that is distinct from insulin-driven regulation of Glut4 in this tissue. We therefore hypothesized that neuronal activity may similarly recruit a glucose transporter to presynaptic surface. While Glut3 is the canonical glucose transporter in neurons (Gerhart et al., 1992), the expression of Glut4 in several brain regions, including the cortex, hippocampus, cerebellum and the olfactory bulb has been reported (Kobayashi et al., 1996; Vannucci et al., 1998). The functional significance of Glut4 in the nervous system, however, has remained unknown. Here we show that Glut4 is present at hippocampal nerve terminals, and we uncover a novel paradigm whereby Glut4 is mobilized by neuronal activity to support the energetic demands of firing synapses. This mobilization relies on an AMP kinase-mediated metabolic feedback to regulate Glut4 delivery in nerve terminals similar to muscle. Finally, we show that acute genetic ablation of Glut4 leads to an arrest of synaptic vesicle recycling, mimicking the deficits seen with glucose deprivation.

RESULTS

Glut4 is Expressed in the Brain and Present at Nerve Terminals

We verified previous reports of Glut4 expression in both cerebellum (Kobayashi et al., 1996; Vannucci et al., 1998) and hippocampus (Fernando et al., 2008; Grillo et al., 2009) using immunohistochemical staining with anti-Glut4 antibody in acute brain slices (Fig. 1A-D). Glut4 is expressed throughout the hippocampus (Fig. 1A) including layers enriched in presynaptic endings, such as stratum radiatum, as indicated by counterstaining against the SV marker vGlut1 (Fig. 1C). In the cerebellum, Glut4 expression is pronounced in the granular layer which contains soma, dendrites and axons (Fig. 1B), but appears to be lower in Purkinje cells (Fig. 1D), consistent with previous observations (Vannucci et al., 1998). To further characterize the subcellular distribution of Glut4 and determine if it is present in nerve terminals, we carried out immunocytochemistry analysis in dissociated rat hippocampal neurons which showed that Glut4 is widely distributed throughout the soma

and dendrites (Fig. 1E) and additionally co-localizes with the abundant presynaptic protein synapsin (Fig. 1F). Neurons in which Glut4 was ablated (by shRNA expression) showed much lower levels of staining (Fig. 1G and H), while neurons overexpressing Glut4 were stained more brightly (Fig. S1A and B) than the control confirming the specificity of Glut4 immunocytochemistry. Thus we conclude that Glut4 is distributed throughout neurons including nerve terminals.

Activity Drives Glut4 to Presynaptic Plasma Membrane

We expressed a pHluorin-tagged variant of Glut4 (Burchfield et al., 2013) in primary neurons (Fig. S2A) to examine its behavior during AP firing which led to a ~2-fold over-expression of Glut4 in nerve terminals (Fig. S2B). Under resting conditions, pHluorin, which was spliced into the first exo-facial loop of Glut4, is expected to be quenched if it resides in an acidic endosomal compartment. Rapid perfusion of a low pH solution which quenches surface pHluorin fluorescence showed that very little Glut4-pHluorin (7.5% of total) resides on the axonal surface under resting conditions (Fig. 2A and D). Perfusion with NH_4Cl at pH 7.4 rapidly equilibrates organelle pH to that of the buffer (Fig. 2A, C and S2A) demonstrating that Glut4-pHluorin (Glut4-pH) primarily resides in an acidic compartment. AP firing led to rapid accumulation of Glut4 on the synaptic surface that persisted for ~ 2 minutes after the end of the stimulus (Fig. 2B and 3C). We verified that the increased Glut4-pH signal arose from surface accumulation as it was fully quenched by perfusion of low pH solution (Fig. 2C). On average, persistent AP firing led to a maximal accumulation of ~ 20% of the total pool (i.e. the fluorescence achieved during a prior NH_4Cl perfusion) of Glut4 on the synaptic surface of boutons (Fig. 2D). The time constant of surface Glut4 accumulation during constant AP firing was only ~two times slower than SVs (data not shown), indicating that even a few AP likely recruit Glut4 to the plasma membrane. Indeed, stimulation with 100 AP is sufficient to cause a statistically significant increase in Glut4-pH fluorescence (Fig. 2B, inset), but smaller fluorescence changes with fewer AP would be difficult to detect experimentally. Given previous reports of insulin-mediated regulation of neuronal Glut4 (Fernando et al., 2008; Grillo et al., 2009), we examined the effects of insulin on Glut4 trafficking in hippocampal axons. Consistent with the somatodendritic distribution of the insulin receptor (Abbott et al., 1999), acute insulin treatment failed to affect axonal surface Glut4 levels (Fig. S3A), while it did trigger surface accumulation of Glut4 in somatodendritic compartments (data not shown). Similarly, long-term insulin deprivation did not impact activity-driven presynaptic Glut4 mobilization (Fig. S3B). Thus, like muscle contraction, presynaptic Glut4 mobilization in response to activity is distinct from insulin signaling.

Although previous studies implied that the canonical neuronal glucose transporter Glut3 redistributes to somatic and dendritic cell surface during prolonged activity (Ferreira et al., 2011), expression of a pHluorin-tagged Glut3 (see Methods) showed that under resting conditions virtually all of the expressed Glut3-pH was resident on the axonal surface, and AP firing led to no detectable increase in surface accumulation (Fig. 2E-G). Thus, in axons, Glut3 likely provides a constant source of glucose uptake that is not significantly regulated by activity.

Glut4 Recycling is Distinct from Synaptic Vesicles

We wondered if the intracellular pool of Glut4 vesicles is distinct from that of SVs. To examine this issue we used several approaches, including characterization of the both the biophysical properties of presynaptic Glut4-pH (described here) and the molecular basis of the control of Glut4-pH (described below). We previously developed methods to determine the pH inside organelles harboring pHluorin by monitoring the change in fluorescence resulting from rapid and reversible perfusion of NH_4Cl (Sankaranarayanan et al., 2000). Applying these approaches to Glut4-pH in nerve terminals showed that the average pH of the endosomes harboring Glut4 is ~6.1 (Fig. 3A), more alkaline than typical SVs (~5.5) (*9*). The slow recovery of Glut4-pH following stimulation (Fig. 3B) also differs significantly from typical SV proteins, for which pHluorin-tagged variants are endocytosed and reacidified following exocytosis in ~6 s at 37 °C (Balaji et al., 2008), indicating at the very least they are likely recycled by different molecular mechanisms. Co-expression of Glut4-pH and vGlutmOrange2 (vGlut-mO) allowed us to examine the recycling behavior of the two proteins simultaneously after a stimulus. We found that Glut4-pH recovers with a $t_{1/2}$ ~ 20 times slower that SVs (Fig. 3B and C). Finally, the maximal fraction of Glut4-pH driven to the surface by electrical activity (~20%, Fig. 2D) is much smaller than that for SVs (~45%) (Kim and Ryan, 2010). These data all suggest that although Glut4 is driven to undergo exocytosis at nerve terminals by AP firing, it likely does so from an endosomal compartment that is distinct from SVs.

Glut4 is Required for Sustained Synaptic Function

We tested the idea that insertion of Glut4 during activity is critical for energetic support of SV endocytosis, which is blocked in the absence of stimulated glycolysis (Rangaraju et al., 2014). We examined the kinetics of SV recycling using vGlut-pH in neurons in which expression of Glut4 was ablated using shRNA-mediated knockdown (Fig. 1G-H, and S1B). We found that following co-expression of the shRNA targeting Glut4 and vGlut-pH, resting ATP levels were not significantly changed (Fig. S4A). About one third (9/26) of neurons had a high resting fluorescence and no longer elicited any exocytic response (not shown). The remaining neurons had normal exocytosis in the absence of Glut4 (Fig. 4A and D) but showed a dramatic arrest of endocytosis and reacidification (Fig. 4A and C). Perfusion of low pH solution after AP firing (Fig. 4B) indicated that virtually all of the elevated post-stimulus vGlut-pH fluorescence could be quenched, confirming that loss of Glut4 in neurons leads to an arrest of SV endocytosis, a defect that is very similar to that observed following acute blockade of glycolysis (Rangaraju et al., 2014). Re-expressing an shRNA-insensitive variant of Glut4 in the KD neurons fully restored SV recycling (Fig. 4A and C). It is possible that the requirement for Glut4 in SV recycling is unrelated to its function as a glucose transporter. We tested this hypothesis by introducing a point mutation (E329Q) in a region of Glut4 that is conserved between this transporter and Glut1, in which this mutation inactivates the transport function, locking Glut1 in an inward-facing conformation (Deng et al., 2014). The transport-deficient Glut4-pHluorin showed very similar behavior to the wildtype form during AP firing, accumulating on the axonal and presynaptic surface (Fig. 5A and B). However expression of transport-deficient Glut4-RFP failed to rescue SV recycling in Glut4 KD neurons (Fig. 5C), even though this mutant was still able to rapidly

insert into the plasma membrane during activity. Thus the presence of a functional transporter on the synaptic surface is required for sustained SV recycling.

We wondered if this acute reliance on new glucose uptake would be mitigated during more modest levels of activity. Although endocytosis of SVs is blocked in dGlu following 100 AP stimuli, we found that the defect is much more modest for smaller numbers of stimuli (Fig. 6A and C). Similar to full glycolytic block, we found that SV endocytosis was much more dramatically impacted in Glut4 KD for stimuli of 100 AP compared to smaller stimuli (Fig. 6B and C). These experiments reveal that in the absence of glycolysis, there is sufficient reserve ATP to handle a brief burst of activity but that synapses rely on the acute delivery of Glut4 to the axonal surface to sustain function when more than ~ 10 AP are fired in a short period of time.

AMP Kinase Mediates Glut4 Mobilization during Activity

Exercise-driven mobilization of Glut4 in muscle is driven by activation of AMP kinase (AMPK) as a result of a transient change in the AMP (or ADP) to ATP ratio (Fryer et al., 2002; Kurth-Kraczek et al., 1999; Mu et al., 2001) and this enzyme has also been shown to be activated in neurons by AP firing (Sample et al., 2015). We present three key pieces of evidence to support the idea Glut4 mobilization in axons is controlled by AMPK. First, we found that acute application of the AMPK activator AICAR (Merrill et al., 1997) led to a rapid increase in Glut4-pH signal in axons but did not trigger mobilization of SVs (Fig. 7A, right). We verified that the increased Glut4-pH signal was due surface accumulation of Glut4 through exocytosis as it was fully quenched by perfusion of low pH solution (Fig. 7A, left). Thus activation of AMPK alone can drive Glut4 exocytosis at nerve terminals from an internal endosomal compartment distinct from SVs. Second, in order to determine if an AMPK pathway is engaged during AP firing, we examined the impact of inhibiting AMPK on Glut4 mobilization during electrical activity. Blockade of AMPK using the AMPK inhibitor dorsomorphin (Zhou et al., 2001) or expression of the catalytically inactive α subunit of AMPK (Woods et al., 2000) significantly reduced activity-driven Glut4 translocation (Fig. 7B and C). Dorsomorphin also blunted AICAR-mediated Glut4 translocation (Fig. S5A), validating its inhibitory effects on AMPK. In agreement with previous results in muscle (Mu et al., 2001), AMPK inhibition only partially blunted Glut4 mobilization suggesting that other regulatory factors, such as the elevation of intracellular calcium during activity, may also contribute to Glut4 recruitment. Third, expression of a constitutively dephosphorylated form of the Rab GAP protein TBC1D1 (TBPC1D1-3A: S621, S231 and T499 mutated to alanine), a critical target of AMPK that regulates Glut4 translocation in muscle (Vichaiwong et al., 2010), significantly slowed activity-driven exocytosis of Glut4 at nerve terminals (Fig. 7D and E). In contrast, expression of AS160, an adipocyte isoform of TBC1D1 in which Akt phosphorylation sites downstream of insulin signaling were mutated (Sano et al., 2003), did not affect activity-driven Glut4 trafficking (data not shown). These data together support the idea that activation of the metabolic sensor AMPK is the primary driver of Glut4 exocytosis at nerve terminals. AMPK does not, however, regulate SV exocytosis as neither dorsomorphin nor TBC1D1-3A had any impact on exocytosis of vGlut-pH (Fig. S5D and E), despite their inhibitory effects on Glut4 mobilization. Given the arrest of SV recycling in Glut4 KD neurons (Fig. 4), we reasoned

that blunting AMPK-driven Glut4 translocation would similarly slow SV endocytosis for large stimuli. Although dorsomorphin treatment or TBC1D1-3A expression alone only partially impaired Glut4 translocation (Fig. 7B-E), when combined their affects were additive (Fig. S5B and C). Under these conditions, SV endocytosis following a large stimulus slowed significantly (Fig. 7F). Thus, we conclude that AMPK-driven Glut4 exocytosis is essential for proper synaptic function.

Glut4 and synaptic vesicles use distinct pathways of exocytosis

Our finding that AMPK specifically drives exocytosis of Glut4 vesicles but not SVs (Fig. 7) suggests that Glut4 and SVs may use distinct exocytic machinery. To address this, we examined the effects of known blockers of SV exocytosis on Glut4 trafficking. An important consideration however in examining the molecular basis of Glut4 exocytosis is that perturbations that impact SV cycling might lessen the activation of AMP Kinase, since SV recycling is one of the major consumers of ATP in nerve terminals (Rangaraju et al., 2014). We therefore examined both how a given molecular regulator impacts electrical-activity-driven and AICAR-driven Glut4 exocytosis. First, we expressed the tetanus-toxin light chain (TeNT-LC) to cleave the SNARE protein VAMP2 that fully eliminate SV exocytosis (Gaisano et al., 1994), and found that Glut4 mobilization by electrical activity and AICAR were similarly blocked (Fig. 8A and C). Therefore, consistent with previous findings in muscle (Randhawa et al., 2000), VAMP2 is required for presynaptic Glut4 exocytosis. Second, we used shRNA to ablate Munc13 expression, a SNARE-associated protein required for both evoked and spontaneous SV release (Varoqueaux et al., 2002), to completely block SV exocytosis (Fig. S6A). In contrast to SVs, activity-driven mobilization of Glut4 persisted, albeit at lower levels, in Munc13 KD neurons (Fig. 8B and C). Significantly, exocytosis of Glut4 in response to AICAR was completely unaffected by Munc13 removal (Fig. 8B and C), indicating that Glut4 vesicles, unlike SVs, do not require Munc13 for exocytosis. We attribute the decrease in Glut4 mobilization in firing Munc13 KD neurons to the reduced energy burden in these neurons as elimination of SV cycling significantly lowers ATP consumption, and consequently AMPK activation during activity. It is interesting to note that the earliest phase of AP-driven exocytosis of Glut4 is not altered by the absence of Munc13, suggesting that the initial trigger for exocytosis is either not AMPK-driven, or that some other transient energy burden associated with electrical activity drives the early phase of Glut4 insertion. Overall, these findings demonstrate that Glut4 and SVs utilize distinct pathways for exocytosis during neuronal firing and taken together with the different recycling kinetics (Fig. 3) strongly support the idea that in nerve terminals Glut4 does not reside in SVs.

DISCUSSION

Our data reveal a new and important principle of metabolic regulation of presynaptic function: similar to exercising-muscle, “exercising” axons also rely on translocation of the Glut4 glucose transporter to the plasma membrane for metabolic homeostasis. While previous studies investigated potential regulation of neuronal Glut4 by insulin (Fernando et al., 2008; Grillo et al., 2009), we uncovered a novel metabolic role for Glut4 at synapses that more closely resembles its function in muscle than adipocytes. We also show that like

muscle, activity-driven mobilization of Glut4 at synapses is distinct from activation of insulin signaling. In the future, it will be interesting to examine how insulin affects Glut4 trafficking in soma and dendrites, and how Glut4 in turn may regulate post-synaptic function. Similar to neurons, membrane depolarization in muscle, even in the absence of contraction, can drive Glut4 mobilization (Wijesekara et al., 2006), suggesting that in both systems electrical stimulation may be sufficient for AMPK activation.

At present, the identity and molecular composition of presynaptic Glut4 vesicles remains unknown but 4 types of experiments strongly suggest that they are distinct from synaptic vesicles. First, the average pH of the presynaptic Glut4-bearing compartment is more alkaline than that of SVs (Fig. 3A). Second, following exocytosis, Glut4 endocytosis proceeds more slowly than SVs (Fig. 3B and C). Third, although direct activation of AMPK drives Glut4 exocytosis, it does not induce SV exocytosis (Fig. 7A). Fourth, unlike its requirement for SVs, exocytosis of Glut4 vesicles does not rely on Munc13 (Fig. 8B and C). Together, these results strongly argue that the activity-regulated Glut4 vesicle pool is distinct from that of SVs.

As a regulatory module, the extent of Glut4 mobilization in boutons is expected to match their energetic needs through a feedback mechanism involving AMPK. Indeed, Glut4 surface recruitment was diminished in Munc13 KD neuron in which the energetic burden of SV recycling was eliminated (Fig. 8B and C). In contrast, activity-driven membrane recruitment of the transport deficient Glut4 mutant was not elevated compared to the control (Fig. 5A and B), even though the energetic demands of SV recycling were not met by this mutant (Fig. 5C). This apparent lack of a feedback loop in the latter case may be due to the limited amount of Glut4 available for recycling (~ 20%) that is already maximally mobilized in control conditions during our stimulation paradigm (600 APs, 10Hz)

Our findings imply that the requirement of Glut4 mobilization is not evident under modest stimulation conditions. Instead, it is a mechanism that is required for sustained function under constant firing, presumably a condition that engages sufficient metabolic imbalance to activate AMPK. Although Glut4 knockout animals survive to adulthood, they suffer from numerous physiological abnormalities, including shortened lifespan (Katz et al., 1995). The consequences of Glut4 ablation on neuronal network function has yet to be assessed, but given the importance of fuel availability for brain function, removal of one pathway is likely compensated by other metabolic pathways. Indeed, loss of Glut4 in cardiac tissue, an organ that requires constant fuel supply, leads to upregulation of Glut1, which only over time results in the development of cardiac hypertrophy (Abel et al., 1999). Our experiments predict that in the absence of any such compensation, loss of Glut4 in the brain would primarily impact circuits that rely on sustained (many seconds) of activity. It is interesting to note that a poorly understood but effective treatment for drug-resistant childhood epilepsy relies on nutrient supply from a diet that heavily favors ketogenic rather than glycolytic metabolism (Neal et al., 2008). Given that seizure propagation requires sustained neuronal firing with a heavy reliance on activity-driven glycolysis, it is tempting to speculate that the mechanism of protection offered by ketogenic diets is to dampen circuit activity by allowing a block of vesicle recycling. Our findings demonstrate that a critical metabolic regulatory

module that supports muscle function during acute changes in demand is operational at nerve terminals, potentially opening up new routes for therapeutic intervention.

STAR METHODS

Contact for Reagent and Resource Sharing

Further information and requests for resources and reagents should be directed to and will be fulfilled by the Lead Contact Timothy A. Ryan at taryan@med.cornell.edu.

Experimental Model and Subject Details

Animals—All animal-related experiments were performed in accordance with protocols approved by the Weill Cornell Medicine or Rockefeller University IACUC. Wild-type rats and mice were of the Sprague-Dawley strain (Charles River code 400, RRID: RGD_734476), and CD1 background, respectively.

Primary Neuronal Culture—Hippocampal CA1-CA3 neurons were isolated from 1- to 3-day-old rats of mixed gender, plated on polyornithine-coated coverslips, transfected 7 days after plating, and imaged 14-21 days after plating as previously described (Ryan, 1999). Neurons were maintained in culture media composed of MEM (Thermofisher Scientific S1200038), 0.6% glucose, 0.1 gm/l bovine transferrin (Millipore 616420), 0.25 gm/l insulin, 0.3 gm/l glutamine, 5–10% fetal bovine serum (Atlanta Biologicals S11510), 2% B-27 (Thermofisher Scientific 17504-044), and 4 μm cytosine β-d-arabinofuranoside. Cultures were incubated at 37°C in a 95% air/5% CO2 humidified incubator for 14–21 days prior to use.

Method Details

Plasmid Constructs—The following previously published DNA constructs were used: vGlut-pHluorin (Voglmaier et al., 2006), vGlutmOrange2 (Hoppa et al., 2012), and VAMP-mCherry (Hoppa et al., 2012), Munc13-1/2 shRNA and Syn-ATP (Rangaraju et al., 2014), and TeNT-LC (gift of M. Dong).Glut4-pHluorin was a gift from D. E. James (Burchfield et al., 2013). To construct Glut4-RFP, HA-Glut4 sequence was PCR first amplified from an HA-Glut4-GFP plasmid (gift of T. E. McGraw) and inserted into the Bam H1 and Age1 sites of FCK-Arch –GFP (Chow et al., 2010), a gift of Edward Boyden (Addgene 22217), to replace Arch. mRFP was PCR amplified from pmRFP-LC3 (Kimura et al., 2007), a gift from Tamotsu Yoshimori (Addgene 21075), and inserted into EcoRI and AgeI sites of Glut4-eGFP. The transport-deficient Glut4-RFP was generated based on the structure of Glut1 (Deng et al., 2014), where E329Q mutation in a region conserved between Glut1 and Glut4 locks the transporter in an inward-facing conformation. Mutagenesis was performed with the QuickChange site-directed mutagenesis kit (Stratagene, Agilent Technologies). Similarly, AMPKα1, a gift from Morris Birnbaum (Addgene 27297) was used for site-directed mutagenesis to generate dominant negative AMPKα1 (D159A). AMPK phosphorylation sites (S237, T505, and S627) (Vichaiwong et al., 2010) in TBC1D1 (gift of G. E. Leinhard) were mutated to alanine using Gibson assembly (New England Biolabs).

To construct Glut3-pH, pHluorin sequence of vGlut-pH was PCR amplified along with the linker sequence encoding SGSTSGGSGGTG and inserted into the first extracellular loop of human Glut3 (gift of G. Bell) between amino acids 50/51 using Gibson assembly. The resultant Glut3-pH piece was PCR amplified and inserted into BamH1 and EcoRI sites of FCK-Arch –GFP. The shRNA targeting rat Glut4 (TR709372A) was purchased from Origene Technologies.

Live Imaging of Neurons—Unless otherwise indicated, all imaging experiments were performed on a custom-built laser illuminated epifluorescence microscope with an Andor iXon+ camera (model #DU-897E-BV). Acousto-optic tunable filters were used to shutter solid state 488 nm and 532 nm lasers. Images were acquired through a 40 × 1.3 NA Fluar Zeiss objective. Luminescence imaging of the presynaptic ATP reporter, Syn-ATP, was performed as previously described (Rangaraju et al., 2014). Coverslips were mounted in a laminar flow perfusion chamber and perfused at 37 °C with Tyrodes buffer containin g (in mM) 119 NaCl, 2.5 KCl, 2 $CaCl_2$, 2 $MgCl_2$, 50 HEPES (pH 7.4), 5 glucose, supplemented with 10 μM 6-cyano-7nitroquinoxalibe-2, 3-dione (CNQX), and 50 μM D,L-2-amino-5phosphonovaleric acid (APV) (both from Sigma) to suppress post-synaptic responses. Action potentials were evoked in neurons with 1 ms pulses creating field potentials of ~10 V/cm via platinum–iridium electrodes.

In deoxyglucose experiments, glucose in the Tyrodes buffer was replaced with 5 mM deoxyglucose. NH_4Cl solution for alkalization of pHluorin-containing vesicles had a similar composition as Tyrodes buffer except it contained (in mM): 50 NH_4Cl and 69 NaCl. The MES solution for acid quench of pHluorin, contained MES in place of HEPES and was set to pH 5.5. Insulin deprivation prior to acute insulin treatment or electrical stimulation was achieved by culturing neurons at days after plating 14-16 for 24-48 hours with media containing insulin-free B27 (ThermoFisher Scientific A1895601).

5-Aminoimidazole-4-carboxamide ribonucleotide (AICAR) purchased from Abcam Biochemicals, and dorsomorphin (compound C) purchased from Sigma-Aldrich, were diluted in Tyrodes buffer to 1 mM and 10 μM, respectively, and applied to neurons. Dorsomorphin was dissolved in DMSO to make a 1 mM stock solution. Neurons were incubated with Tyrodes containing Dorsomorphin for 25-30 minutes and the solution was replaced every 10 minutes without continuous perfusion.

Glut4-pH Measurements—Vesicle pH in Glut4-pH-containing vesicles was calculated as previously described (Sankaranarayanan et al., 2000) and surface fraction of Glut4-pH before and after electrical stimulation was determined using the calculated pH value of 6.06. Maximal $\Delta F/\Delta F_{NH4Cl}$ of Glut4-pH after stimulation was calculated by averaging 10 data points leading up to the peak. Since overexpression of DN AMPKα1 lowered ΔF_{NH4Cl} of Glut4-pH, to calculate maximal $\Delta F/\Delta F_{NH4Cl}$ in Fig. 4C, maximal $\Delta F/F_{initial}$ for each cell, control or overexpressing, was divided by the average $\Delta F_{NH4Cl}/ F_{initial}$ obtained from many control cells (which normalizes for expression level differences of control and DN AMPKα1).

Brain Slice Immunohistochemistry—Adult mouse brain was dissected after cardiac perfusion, post-fixed in 4% PFA/PBS overnight at 4°C, th en cryopreserved in 10% sucrose/PBS for 2 days at 4°C. 20μm frozen sections were cut on a cryostat, coronally for hippocampal regions and sagittally for cerebellar regions. Sections were permeablized with 0.05% Triton X-100/PBS, neutralized with 0.3M Glycine/0.05% Triton X-100/PBS, blocked and stained in 3% donkey serum/0.05% Triton X-100/PBS. The following primary antibodies were used: rabbit anti-Glut4 antibody (Alomone Labs AGT-024, RRID: AB_2631197), guinea pig anti-vGlut1 (Millipore AB5905, RRID: AB_2301751), mouse anti-Calbindin (SWANT C9638, RRID: AB_2314070). The secondary antibodies were: donkey anti-rabbit Alexa568, donkey-anti-guinea pig Alexa488, donkey-anti-mouse Alexa488, and Hoechst for nuclear counterstaining.

Dissociated Neuron Immunocytochemistry—Neurons were fixed with 4% paraformaldehyde, permeabilized with 0.2% Triton X-100, blocked with 5% BSA, and incubated with rabbit anti-Glut4 antibody (see above) and guinea pig anti-synapsin 1/2 (Synaptic Systems 106-004, RRID: AB_1106784), or chicken anti-GFP (ThermoFisher Scientific A10263, RRID: AB_2534024) antibodies, followed by incubation with Alexa 546 or Alexa 568 and Alexa 488 secondary antibodies. Images were collected on Zeiss LSM 510 and LSM 880 confocal microscopes.

Validation of Glut4 knockdown by Immunostaining—Following transfection with vGlut-pH and Glut4 shRNA or Glut4-pH, neurons were fixed and stained with anti-Glut4 antibody and anti-GFP antibody which also recognizes pHluorin. Glut4 expression level was determined by selecting ROIs corresponding to the soma of neurons expressing vGlut-pH or Glut4-pH and measuring the fluorescence intensity of Glut4 immunofluorescence at the ROIs, followed by background subtraction (F_{trans}). The expression level of Glut4 in boutons expressing Glut4-pH was determined by selecting ROIs positive for synapsin I staining. Glut4 immunofluorescence was similarly measured in neighboring untransfected neurons ($F_{untrans}$) in the same illumination field, and the change in expression level was calculated as $F_{trans}/F_{untrans}$ *100% for both Glut4 KD and Glut4 OE.

Quantification and Statistical Analysis

Image Analysis and Statistics—Images were analyzed using the Image J plugin Time Series Analyzer V3 where 10-20 regions of interest (ROIs) of ~2 μm corresponding to responding synaptic boutons were selected and the fluorescence was measured over time. All fitting was done with OriginPro v8 as previously described (Balaji and Ryan, 2007). Statistical analysis was performed with OriginPro v8 and GraphPad Prism v6.0 for PC. In most experiments, the Mann–Whitney U test was used to determine the significance of the difference between two conditions. For paired comparison of responses before and after treatment with dorsomorphin, the Kolmogorov-Smirnov test was used. $P < 0.05$ was considered significant and denoted with a single asterisk, whereas $P < 0.01$, $P<0.001$ and $P < 0.0001$ are denoted with two, three, and four asterisks, respectively. The n value, indicated in the figure legends for each experiment, represents the number of cells imaged.

Quantification of Synaptic Vesicle Endocytic Block—The block in endocytosis of vGlut-pH in Glut4 KD neurons or neurons treated with dGlu was quantified with varying stimulation intensities. For dGlu treatments, the fraction of vGlut-pH signal remaining at two endocytic constants (2τ) at the end of electrical stimulation, denoted as $\Delta F_{2\tau}/\Delta F_{max}$, was determined for each neuron before and after treatment using the τ of before treatment at each stimulation intensity. Endocytic block was calculated as $(\Delta F_{2\tau}/\Delta F_{max})_{after}/(\Delta F_{2\tau}/\Delta F_{max})_{before}$. In the case of Glut4 KD neurons, $\Delta F_{2\tau}/\Delta F_{max}$ was calculated using average τ of control neurons for each stimulation intensity. Endocytic block for each Glut4 KD neuron was measured as:

$$x=\frac{(\Delta F_{2\tau}/\Delta F_{max})_{Glut4KD}}{\mathrm{mean}(\Delta F_{2\tau}/\Delta F_{max})_{control}}$$

The standard error for endocytic block of Glut4 KD was determined as follows:

$$s.e.m=\frac{\sqrt{\sum_{i=1}^{n}{S_{x_i}}^2}}{\sqrt{n}},\qquad S_{x_i}=x.S_{control}$$

Where S_{x_i}, the standard deviation for each value of endocytic block, and $S_{control}$ is the standard deviation of $(\Delta F_{2\tau}/\Delta F_{max})_{control}$ values.

Supplementary Material

Refer to Web version on PubMed Central for supplementary material.

ACKNOWLEDGMENTS

We thank members of the Ryan laboratory, Jeremy Dittman and Tim McGraw for their valuable suggestions and input on this work. We thank David James (U. of Sydney) for providing us with the Glut4-pH construct, Gus Leinhard (Dartmouth U.) for the TBC1D1 construct and G. Bell (U. Chicago) for the Glut3 construct. This work was supported by a grant to TAR from the NIH (NS036942).

REFERENCES

Abbott MA, Wells DG, Fallon JR. The insulin receptor tyrosine kinase substrate p58/53 and the insulin receptor are components of CNS synapses. J Neurosci. 1999; 19:7300–7308. [PubMed: 10460236]

Abel ED, Kaulbach HC, Tian R, Hopkins JC, Duffy J, Doetschman T, Minnemann T, Boers ME, Hadro E, Oberste-Berghaus C, et al. Cardiac hypertrophy with preserved contractile function after selective deletion of GLUT4 from the heart. J Clin Invest. 1999; 104:1703–1714. [PubMed: 10606624]

Balaji J, Armbruster M, Ryan TA. Calcium control of endocytic capacity at a CNS synapse. J Neurosci. 2008; 28:6742–6749. [PubMed: 18579748]

Balaji J, Ryan TA. Single-vesicle imaging reveals that synaptic vesicle exocytosis and endocytosis are coupled by a single stochastic mode. Proc Natl Acad Sci U S A. 2007; 104:20576–20581. [PubMed: 18077369]

Burchfield JG, Lu J, Fazakerley DJ, Tan SX, Ng Y, Mele K, Buckley MJ, Han W, Hughes WE, James DE. Novel systems for dynamically assessing insulin action in live cells reveals heterogeneity in the insulin response. Traffic. 2013; 14:259–273. [PubMed: 23252720]

Chauveau MA, Kaufmann M. Experiences pour la determination du coefficient de l'activite nutritive et repiratoire des muscles en repos et en travail. Comptes Rendus de l'Academie des Sciences. 1887; 104:1126–1132.

Chow BY, Han X, Dobry AS, Qian X, Chuong AS, Li M, Henninger MA, Belfort GM, Lin Y, Monahan PE, et al. High-performance genetically targetable optical neural silencing by light-driven proton pumps. Nature. 2010; 463:98–102. [PubMed: 20054397]

Deng D, Xu C, Sun P, Wu J, Yan C, Hu M, Yan N. Crystal structure of the human glucose transporter GLUT1. Nature. 2014; 510:121–125. [PubMed: 24847886]

Douen AG, Ramlal T, Rastogi S, Bilan PJ, Cartee GD, Vranic M, Holloszy JO, Klip A. Exercise induces recruitment of the "insulin-responsive glucose transporter". Evidence for distinct intracellular insulin- and exercise-recruitable transporter pools in skeletal muscle. J Biol Chem. 1990; 265:13427–13430. [PubMed: 2199436]

Fernando RN, Albiston AL, Chai SY. The insulin-regulated aminopeptidase IRAP is colocalised with GLUT4 in the mouse hippocampus--potential role in modulation of glucose uptake in neurones? Eur J Neurosci. 2008; 28:588–598. [PubMed: 18702730]

Ferreira JM, Burnett AL, Rameau GA. Activity-dependent regulation of surface glucose transporter-3. J Neurosci. 2011; 31:1991–1999. [PubMed: 21307237]

Fryer LG, Foufelle F, Barnes K, Baldwin SA, Woods A, Carling D. Characterization of the role of the AMP-activated protein kinase in the stimulation of glucose transport in skeletal muscle cells. Biochem J. 2002; 363:167–174. [PubMed: 11903059]

Gaisano HY, Sheu L, Foskett JK, Trimble WS. Tetanus toxin light chain cleaves a vesicle-associated membrane protein (VAMP) isoform 2 in rat pancreatic zymogen granules and inhibits enzyme secretion. J Biol Chem. 1994; 269:17062–17066. [PubMed: 7516331]

Gerhart DZ, Broderius MA, Borson ND, Drewes LR. Neurons and microvessels express the brain glucose transporter protein GLUT3. Proc Natl Acad Sci U S A. 1992; 89:733–737. [PubMed: 1731347]

Grillo CA, Piroli GG, Hendry RM, Reagan LP. Insulin-stimulated translocation of GLUT4 to the plasma membrane in rat hippocampus is PI3-kinase dependent. Brain Res. 2009; 1296:35–45. [PubMed: 19679110]

Hoppa MB, Lana B, Margas W, Dolphin AC, Ryan TA. alpha2delta expression sets presynaptic calcium channel abundance and release probability. Nature. 2012; 486:122–125. [PubMed: 22678293]

Ikemoto A, Bole DG, Ueda T. Glycolysis and glutamate accumulation into synaptic vesicles. Role of glyceraldehyde phosphate dehydrogenase and 3-phosphoglycerate kinase. J Biol Chem. 2003; 278:5929–5940. [PubMed: 12488440]

Jang S, Nelson JC, Bend EG, Rodríguez-Laureano L, Tueros FG, Cartagenova L, Underwood K, Jorgensen EM, Colón-Ramos DA. Glycolytic Enzymes Localize to Synapses under Energy Stress to Support Synaptic Function. Neuron. 2016; 90:278–291. [PubMed: 27068791]

Katz EB, Stenbit AE, Hatton K, DePinho R, Charron MJ. Cardiac and adipose tissue abnormalities but not diabetes in mice deficient in GLUT4. Nature. 1995; 377:151–155. [PubMed: 7675081]

Kim SH, Ryan TA. CDK5 serves as a major control point in neurotransmitter release. Neuron. 2010; 67:797–809. [PubMed: 20826311]

Kimura S, Noda T, Yoshimori T. Dissection of the autophagosome maturation process by a novel reporter protein, tandem fluorescent-tagged LC3. Autophagy. 2007; 3:452–460. [PubMed: 17534139]

Knull HR, Fillmore SJ. Glycolytic enzyme levels in synaptosomes. Comp Biochem Physiol B. 1985; 81:349–351. [PubMed: 2990810]

Kobayashi M, Nikami H, Morimatsu M, Saito M. Expression and localization of insulin-regulatable glucose transporter (GLUT4) in rat brain. Neurosci Lett. 1996; 213:103–106. [PubMed: 8858619]

Kurth-Kraczek EJ, Hirshman MF, Goodyear LJ, Winder WW. 5′ AMP-activated protein kinase activation causes GLUT4 translocation in skeletal muscle. Diabetes. 1999; 48:1667–1671. [PubMed: 10426389]

Lauritzen HP, Galbo H, Toyoda T, Goodyear LJ. Kinetics of contraction-induced GLUT4 translocation in skeletal muscle fibers from living mice. Diabetes. 59:2134–2144.

Merrill GF, Kurth EJ, Hardie DG, Winder WW. AICA riboside increases AMP-activated protein kinase, fatty acid oxidation, and glucose uptake in rat muscle. Am J Physiol. 1997; 273:E1107–1112. [PubMed: 9435525]

Mu J, Brozinick JT, Valladares O, Bucan M, Birnbaum MJ. A role for AMP-activated protein kinase in contraction- and hypoxia-regulated glucose transport in skeletal muscle. Mol Cell. 2001; 7:1085–1094. [PubMed: 11389854]

Neal EG, Chaffe H, Schwartz RH, Lawson MS, Edwards N, Fitzsimmons G, Whitney A, Cross JH. The ketogenic diet for the treatment of childhood epilepsy: a randomised controlled trial. Lancet Neurol. 2008; 7:500–506. [PubMed: 18456557]

Randhawa VK, Bilan PJ, Khayat ZA, Daneman N, Liu Z, Ramlal T, Volchuk A, Peng XR, Coppola T, Regazzi R, et al. VAMP2, but not VAMP3/cellubrevin, mediates insulin-dependent incorporation of GLUT4 into the plasma membrane of L6 myoblasts. Mol Biol Cell. 2000; 11:2403–2417. [PubMed: 10888677]

Rangaraju V, Calloway N, Ryan TA. Activity-driven local ATP synthesis is required for synaptic function. Cell. 2014; 156:825–835. [PubMed: 24529383]

Roy D, Marette A. Exercise induces the translocation of GLUT4 to transverse tubules from an intracellular pool in rat skeletal muscle. Biochem Biophys Res Commun. 1996; 223:147–152. [PubMed: 8660361]

Ryan TA. Inhibitors of myosin light chain kinase block synaptic vesicle pool mobilization during action potential firing. J Neurosci. 1999; 19:1317–1323. [PubMed: 9952409]

Sample V, Ramamurthy S, Gorshkov K, Ronnett GV, Zhang J. Polarized activities of AMPK and BRSK in primary hippocampal neurons. Mol Biol Cell. 2015; 26:1935–1946. [PubMed: 25788287]

Sankaranarayanan S, De Angelis D, Rothman JE, Ryan TA. The use of pHluorins for optical measurements of presynaptic activity. Biophys J. 2000; 79:2199–2208. [PubMed: 11023924]

Sano H, Kane S, Sano E, Mîinea CP, Asara JM, Lane WS, Garner CW, Lienhard GE. Insulin-stimulated phosphorylation of a Rab GTPase-activating protein regulates GLUT4 translocation. J Biol Chem. 2003; 278:14599–14602. [PubMed: 12637568]

Vannucci SJ, Koehler-Stec EM, Li K, Reynolds TH, Clark R, Simpson IA. GLUT4 glucose transporter expression in rodent brain: effect of diabetes. Brain Res. 1998; 797:1–11. [PubMed: 9630471]

Varoqueaux F, Sigler A, Rhee JS, Brose N, Enk C, Reim K, Rosenmund C. Total arrest of spontaneous and evoked synaptic transmission but normal synaptogenesis in the absence of Munc13-mediated vesicle priming. Proc Natl Acad Sci U S A. 2002; 99:9037–9042. [PubMed: 12070347]

Vichaiwong K, Purohit S, An D, Toyoda T, Jessen N, Hirshman MF, Goodyear LJ. Contraction regulates site-specific phosphorylation of TBC1D1 in skeletal muscle. Biochem J. 2010; 431:311–320. [PubMed: 20701589]

Voglmaier SM, Kam K, Yang H, Fortin DL, Hua Z, Nicoll RA, Edwards RH. Distinct endocytic pathways control the rate and extent of synaptic vesicle protein recycling. Neuron. 2006; 51:71–84. [PubMed: 16815333]

Wijesekara N, Tung A, Thong F, Klip A. Muscle cell depolarization induces a gain in surface GLUT4 via reduced endocytosis independently of AMPK. Am J Physiol Endocrinol Metab. 2006; 290:E1276–1286. [PubMed: 16418206]

Woods A, Azzout-Marniche D, Foretz M, Stein SC, Lemarchand P, Ferré P, Foufelle F, Carling D. Characterization of the role of AMP-activated protein kinase in the regulation of glucose-activated gene expression using constitutively active and dominant negative forms of the kinase. Mol Cell Biol. 2000; 20:6704–6711. [PubMed: 10958668]

Zhou G, Myers R, Li Y, Chen Y, Shen X, Fenyk-Melody J, Wu M, Ventre J, Doebber T, Fujii N, et al. Role of AMP-activated protein kinase in mechanism of metformin action. J Clin Invest. 2001; 108:1167–1174. [PubMed: 11602624]

HIGHLIGHTS

- The glucose transporter Glut4 is present at nerve terminals.
- Neuronal activity recruits Glut4 to presynaptic plasma membrane.
- Glut4 is required for synaptic function during sustained activity.
- AMP kinase drives Glut4 mobilization during activity.

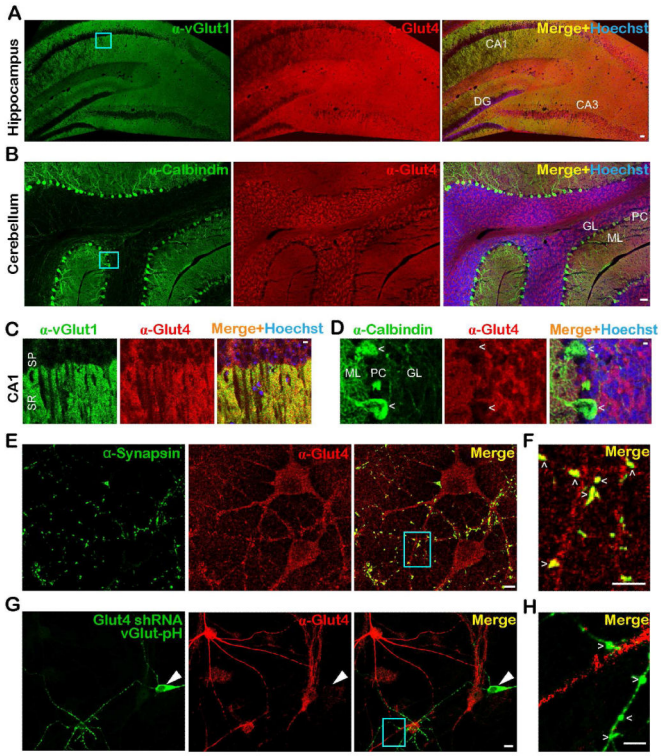

Figure 1. The glucose transporter Glut4 is expressed in the brain and is present at nerve terminals

(A-D) Immunohistochemical staining of adult mouse brain slices with antibodies against Glut4 (red), and (A, C) the presynaptic marker vGlut1, or (B, D) the Purkinje cell marker calbindin (green). Hoechst nuclear staining is shown in blue. Enlarged images of the cyan boxes in A and B show that (C) Glut4 is enriched in the synaptic-rich stratum radiatum, and (D) expressed at lower levels in Purkinje cells (arrowhead). DG, dentate gyrus; GL, granule layer; ML, molecular layer; PC: Purkinje cells; SP, stratum pyramidale; SR, stratum radiatum. CA1 and CA3 are hippocampal regions. (E-G) Immunostaining of dissociated rat hippocampal neurons with antibodies against Glut4 (red) and (E, F) the presynaptic marker synapsin, or (G) pHluorin/GFP of vGlut-pH (green) in neurons expressing Glut4 shRNA. (E) Glut4 is broadly expressed in somato-dendritic regions, (F) but also co-localizes with synapsin at nerve terminals (arrowheads) as shown in the enlarged image of the cyan box in D. (G-H) Glut4 immunofluorescence is reduced (by 70%, see STAR Methods) in neurons transfected with Glut4 shRNA and vGlut-pH, indicating the specificity of Glut4 antibody. (G) Large arrowheads point to the soma and (H) small arrowheads to boutons of the transfected neuron. Scale bars: (A, B) 50 μm, (C-H) 5 μm. See also Figure S1.

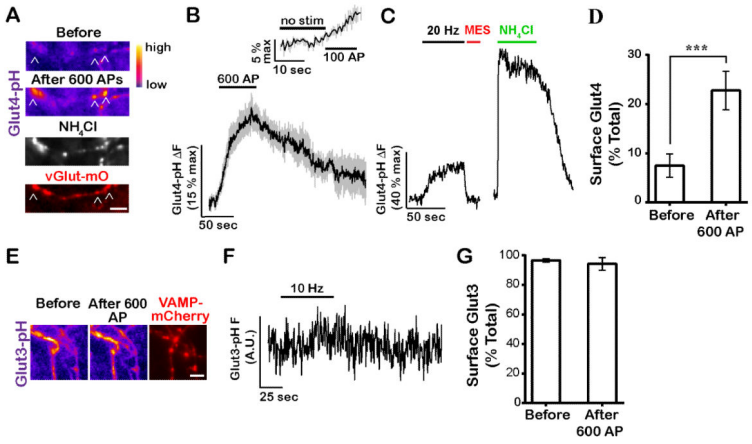

Figure 2. Neuronal firing drives Glut4 vesicles to the presynaptic plasma membrane

(A-D) Neurons expressing Glut4-pH were electrically stimulated with 600 AP. (A) Glut4-pH (pseudocolor) and the synaptic vesicle marker vGlut-mO (red) before and after stimulation. Neutralization of Glut4-pH vesicles with NH_4Cl (white) reveals total axonal pool. (B) Average trace of Glut4-pH (n = 12 cells) with 600 AP-stimulation with the inset showing response after the first 100 AP. ΔF values were normalized to maximal ΔF from NH_4Cl treatment. Error bars are shown in gray and are SEM. (C) a sample trace where stimulation was followed by quenching of extracellular pHluorin with MES acid and neutralization of Glut4-pH vesicles with NH_4Cl. (D) Average surface fraction of Glut4-pH before and after stimulation (% total). Before: 7 ± 2, after 600 AP: 23 ± 4; n = 11 cells. (E-G) Glut3-pH does not mobilize at nerve terminals in response to activity. (E) Pseudocolor images of Glut3-pH in axons co-expressing the synaptic vesicle marker VAMP-mCherry (red) before and after stimulation with 600 AP (10 Hz). (F) Sample trace of Glut3-pH fluorescence (in arbitrary units) in response to stimulation. (G) Average surface fraction of Glut3-pH before and after stimulation (% toal). Before: 97 ± 1, after 600 AP: 94 ± 5; n = 5 cells. Scale bars (A, E), 5 μm. All data are shown as mean ± SEM. See also Figure S2 and S3.

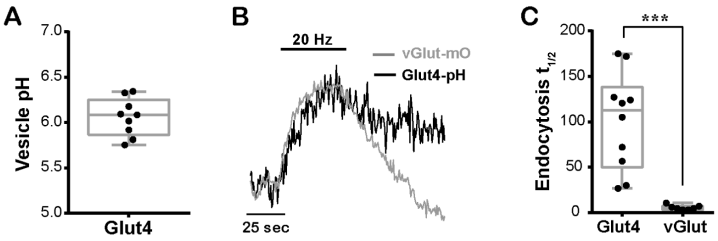

Figure 3. Glut4 vesicles are distinct from synaptic vesicles

(A) The pH of axonal Glut4 vesicle measured from responses to acid quenching and neutralization with NH_4Cl. The box and whisker plot represents median (line), 25^{th}-75^{th} percentile (box), and min-max (whisker). Mean pH: 6.1 ± 0.1; n = 9 cells. (B) Sample traces from boutons co-expressing Glut4-pH and vGlut-mO stimulated with 600 AP (20 Hz). (C) Decay half-time (sec) of Glut4-pH and vGlut-pH (in separate cells) after stimulation with 600 AP (10 Hz): Glut4-pH: 101 ± 17, vGlutpH: 6 ± 1**;** n = 7-10 cells per condition. *** P<0.001.

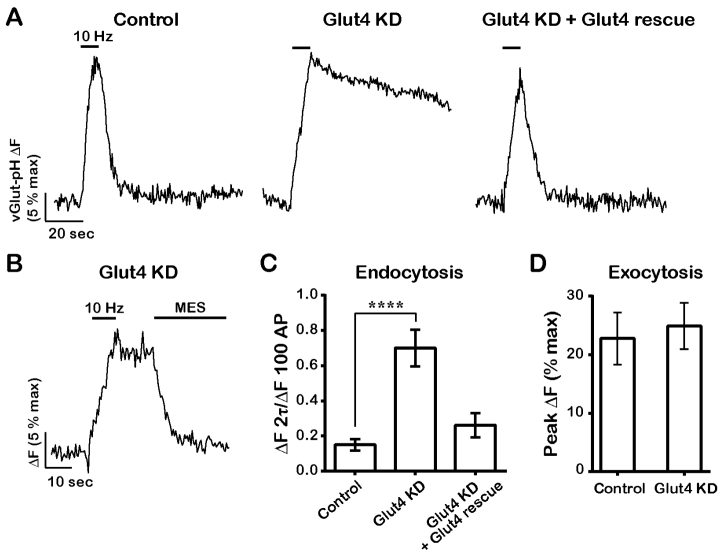

Figure 4. Glut4 is required for synaptic vesicle recycling following bursts of AP firing

(A-D) Sample vGlut-pH traces in response to 100 AP (10 Hz) in (A) control, Glut4 KD, and Glut4 KD neurons expressing shRNA-resistant Glut4-RFP, or (B) in Glut4 KD neurons where stimulation was followed by quenching of extracellular pHluorin with MES acid. (C) Average endocytic block measured as the fraction of vGlut-pH signal remaining at two endocytic time constants (2T) of the control at the end of stimulation. Control: 0.15 ± 0.03, Glut4 KD: 0.7 ± 0.1, rescue: 0.26 ± 0.07; n = 13-17 cells. (D) Average exocytosis of vGlut-pH measured as ΔF at the end of 100 AP normalized to ΔF_{NH4Cl} (% max). Control: 23 ± 4, Glut4 KD: 25 ± 4; n= 13-15 cells. All error bars are SEM. **** P<0.0001. See also Figure S4.

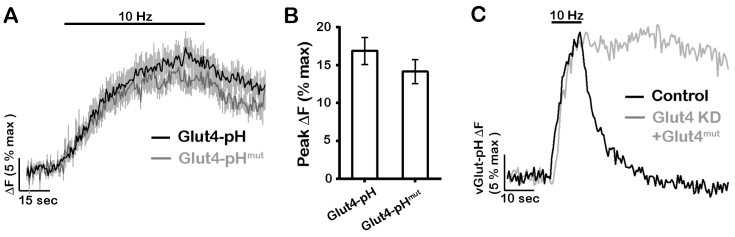

Figure 5. The glucose transport activity of Gut4 is essential for synaptic vesicle recycling

(A-B) Glut4 mutant defective in glucose transport is recruited to synaptic surface similar to wildtype. (A) Average traces of wildtype and mutant Glut4-pH stimulated with 600 AP (10Hz). Error bars are shown in gray. (B) Average peak ΔF of Glut4-pH (% max) in response to 600 AP. Control data are the same as in Fig. 2B. Control: 17 ± 2, Glut4-pH^{mut}: 14 ± 2; n = 6 - 16 cells. (C) Sample vGlut-pH traces in response to 100 AP (10 Hz) in control or Glut4 KD neurons expressing shRNA-resistant Glut4 mutant. All error bars are SEM.

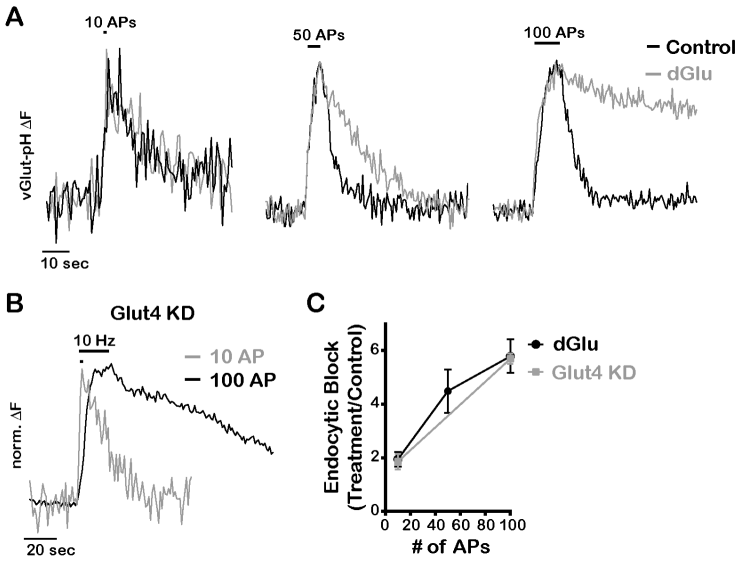

Figure 6. Energetic requirement for glycolysis and glucose uptake increases with duration of activity

(A) Normalized vGlut-pH traces in response to 10, 50 and 100 AP (10Hz) before and 5 min after incubation with dGlu. (B) Normalized vGlut-pH traces of Glut4 KD neurons stimulated with 10 or 100 AP (10 Hz). (C) Average endocytic block for varying AP trains measured as the fraction of the maximal fluorescence remaining after 2 endocytic time constants in treated (dGlu or Glut4 KD) compared to control conditions, n = 4-21 cells per condition. All error bars are SEM.

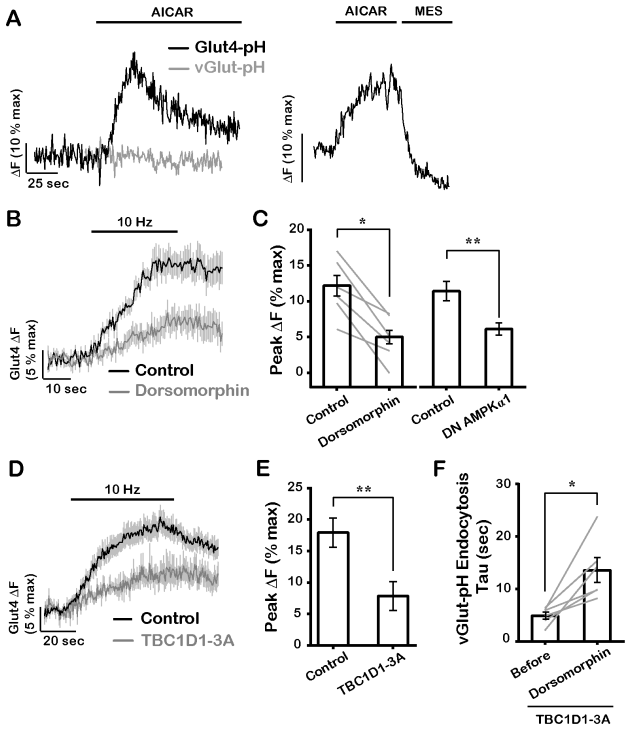

Figure 7. AMP kinase mediates mobilization of Glut4 at presynaptic boutons

(A) Representative responses of (left) Glut4-pH and vGlut-pH to treatment with 1 mM AICAR, or (right) AICAR treatment of Glut4-pH, immediately followed by MES acid quench. (B) Average traces of Glut4-pH stimulated with 300 AP (10 Hz) before and 25 minutes after incubation with 10 μM dorsomorphin, an AMPK inhibitor. (C) Average Glut4 peak ΔF (% max) in response to 300 AP before and after dorsomorphin treatment, or 600 AP with or without expression of dominant negative (DN) AMPKα1. Due to the reduction of ΔF_{max} values with the expression of DN AMPKα1, all ΔF_{max} values were normalized to the control (see Material and Methods). Control: 12 ± 1, dorsomorphin: 5 ± 1, control: 11 ± 1, DN AMPKα1: 5.9 ± 0.8; n = 6-8 cells. (D) Average Glut4-pH traces in response to 600 AP (10 Hz) in control neurons or neurons expressing TBC1D1-3A in which putative AMPK phosphorylation sites were mutated. (E) Average maximal ΔF (% max) in response to 600 AP in control and TBC1D1-3A-expressing neurons. Control data are the same as in Fig. 2B. Control: 18 ± 2, TBC1D1-3A: 8 ± 2; n = 8-12 cells. (F) Endocytosis time constant (sec) of vGlut-pH in neurons expressing TBC1D1-3A, stimulated with 600 AP (10Hz) before and after 30 minutes of dorsomorphin treatment. Before: 4.9 ± 0.7, dorsomorphin: 14 ± 2; n = 6 cells. Error bars in graphs are shown in gray (B and D). All error bars are SEM. * P< 0.05, ** P< 0.01. See also Figure S5.

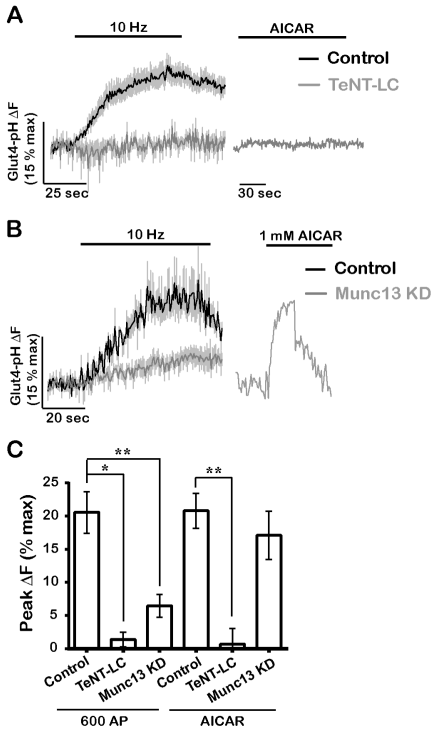

Figure 8. Glut4 and synaptic vesicles use distinct machinery for exocytosis

(A) Expression of tetanus toxin light chain (TeNT-LC) blocks Glut4 exocytosis membrane in response to electrical stimulation (600 AP, 10 Hz) and AICAR treatment. (B) Munc13 KD does not block AICAR-driven Glut4 exocytosis while it only partially inhibits activity-driven exocytosis (600 AP, 10 Hz). (C) Average peak ΔF (% max) in response to 600 AP or AICAR in the same genotypes as shown in A and B. 600 AP (control: 20 ± 3, TeNT-LC: 1 ± 1, Munc13 KD: 6 ± 2); AICAR (control: 20 ± 3, TeNT-LC: 0 ± 2, Munc13 KD: 17 ± 4); n = 3-13 cells. Error bars in graphs are shown in gray (A and B). All error bars are SEM. See also Figure S6.